

# Forced capillary gravity surface waves over a bump – Critical surface tension case

JS Kim<sup>1</sup>SI Whang<sup>2</sup>JW Choi<sup>3</sup>

Received 15 November 2017; revised 13 February 2018

## Abstract

This paper concerns forced surface waves on an incompressible, inviscid fluid in a two-dimensional channel with nonzero surface tension on the free surface and a small bump on a horizontal rigid flat bottom. It is known that if non-dimensional wave speed, called Froude number, is near 1 and a non-dimensional surface tension, called Bond number, is near  $1/3$ , the KdV theory fails and a time dependent fifth order KdV equation, called the Kawahara equation, can be derived to study the wave motion on the free surface. In this paper both time independent and time dependent forms of the Kawahara equation with a forcing are studied numerically and theoretically and various numerical results are presented.

*Keywords:* Forced Kawahara Equation

# 1 Introduction

The capillary-gravity waves on a two-dimensional fluid flow of finite depth have been investigated since nineteenth century. We consider the fluid of constant density, which is incompressible, inviscid and bounded above by a free surface and below by a rigid bottom with a small bump. Let  $h$  and  $C$  be the depth of fluid at infinity and the speed of the flow far upstream, respectively. Let  $\rho$  be the density of the fluid and  $T$  be the surface tension coefficient on the free surface. In this case, the wave on the free surface is determined by two non-dimensional constants: non-dimensional wave speed, called Froude number  $F = C/\sqrt{gh}$ , and non-dimensional surface tension, called Bond number  $\tau = T/(\rho gh^2)$ , where  $g$  is the gravitational constant.

If  $F$  is not near 1, linear theory is applicable [14]. However, for  $F$  near 1, nonlinear theory must be developed. Nonlinear surface waves over a flat bottom (no bump) have been studied experimentally and theoretically. After non-dimensionalizing the problem, a Korteweg-de Vries (KdV) equation, was derived to approximate solutions of the exact equations when Froude number near 1 but Bond number is not near  $1/3$ . ([5, 7, 8, 11, 12, 17] and references therein). However, when shallow fluid is considered, the effect of surface tension should not be neglected. In particular, if  $\tau$  is near  $1/3$ , the formal derivation of the KdV equation is not valid and if  $F = 1 + \lambda_1 \epsilon^2$  and  $\tau = (1/3) + \tau_1 \epsilon$  with  $\epsilon > 0$  a small parameter, then the following model equation, called the Kawahara equation, can be derived [10]

$$\eta_t + \lambda_1 \eta_x - (3/2)\eta\eta_x + (\tau_1/2)\eta_{xxx} - (1/90)\eta_{xxxxx} = 0, \quad (1)$$

$$x \in (-\infty, +\infty), \quad t > 0 \quad .$$

If only steady waves are considered, (1) becomes

$$2\lambda_1 \eta - (3/2)\eta^2 + \tau_1 \eta_{xx} - (1/45)\eta_{xxxx} = 0, \quad x \in (-\infty, +\infty), \quad (2)$$

where  $\eta \rightarrow 0$  as  $x \rightarrow -\infty$ . The solutions of (2) have been extensively studied in [1, 2, 3, 4, 9, 13, 15]. According to the eigenvalues of the corresponding

linearised equation of (2), for different  $\lambda_1$  and  $\tau_1$  the phase spaces of solutions of (2) can be characterised [1, 2, 3, 4, 9, 13, 15].

In this article, we consider steady and unsteady surface waves generated by a small bump placed on a flat bottom to study the effects of variations of bottom surface to the fluid motion in the case that the Froude number  $F$  is near 1 and the Bond number  $\tau$  near  $1/3$ . We assume that  $b(x)$  is a non-dimensional function related to the bump. Then, by a similar derivation, (1) becomes the forced Kawahara equation (F-Kawahara)

$$\eta_t + \lambda_1 \eta_x - (3/2)\eta\eta_x + (\tau_1/2)\eta_{xxx} - (1/90)\eta_{xxxxx} = b_x/2, \quad (3)$$

$$x \in (-\infty, +\infty), \quad t > 0.$$

This paper first considers steady solutions of the F-Kawahara equation (3) theoretically and numerically, i.e, the solutions of the following equation,

$$2\lambda_1 \eta_x - 3\eta\eta_x + \tau_1 \eta_{xxx} - (1/45)\eta_{xxxxx} = b_x, \quad x \in (-\infty, +\infty). \quad (4)$$

Assume that the function  $b(x)$  is even in  $x$  with a semi-circular shape, and if  $\tau_1$  is fixed, then  $\lambda_1 < 0$  is the only parameter that varies. For each large value of  $\lambda_1 < 0$ , there exists one single-hump solution  $\eta_s$  of (4), where the amplitude of  $\eta_s$  is small [6]. The solutions decay to zero exponentially at infinity. Equation (2) has many single or multi-hump solutions [4], which makes one wonder whether there are solutions of (4) near these solutions of (2). A numerical shooting method is used to find the solutions of (4) numerically. If  $\tau_1$  is fixed, we show numerically that there are no solutions of (4) for small  $\lambda_1 < 0$ . Moreover, there exists a cut-off value  $\lambda_0 < 0$  such that for  $\lambda_1 < \lambda_0$  there exist exactly two branches of symmetric single-hump solutions of (4). As  $\lambda_1 < 0$  becomes large, one branch of solutions has small amplitude, which are  $\eta_s$  from the rigorous existence proof [6], while another branch of solutions, denoted by  $\eta_e$ , has large amplitudes, which are near the single-hump solutions obtained in [4]. We also find numerically that there are many multi-hump solutions of (4) for  $\lambda_1 < 0$  not small. The hydraulic fall solutions, which are zero ahead of the bump and period-free behind the

bump, are also found numerically. These hydraulic fall solutions occurs as the limiting solutions of periodic solutions.

Next, for the time-dependent equation (3), we consider the initial value problem (IVP) of equation (3) with an initial condition  $\eta(\mathbf{x}, 0) = \eta_0(\mathbf{x})$ .

Using (3) with  $\eta(\mathbf{x}, 0)$  we find numerically that the solution  $\eta_s$  of (4) is numerically stable and the large single-hump solution  $\eta_\ell$  is unstable under nonzero small perturbations. We also show numerically that hydraulic fall solutions are stable but multi-hump solutions of (4) are unstable.

## 2 Derivation of approximate model equations

We consider two-dimensional capillary-gravity surface waves on a fluid flow of constant density. The fluid is assumed to be incompressible and inviscid, and bounded above by a free surface and below by a bump of compact support on a rigid horizontal bottom.

The Cartesian coordinate  $(\mathbf{x}^*, \mathbf{y}^*)$  is chosen such that  $\mathbf{x}^*$ -axis is aligned along the longitudinal direction and  $\mathbf{y}^*$ -axis is the vertical direction opposite to the gravity. Then the governing equations and boundary conditions of the fluid motion are [14]: in the fluid region,

$$\begin{aligned} \mathbf{u}_{\mathbf{x}^*}^* + \mathbf{v}_{\mathbf{y}^*}^* &= 0, & \mathbf{u}_{\mathbf{t}^*}^* + \mathbf{u}^* \mathbf{u}_{\mathbf{x}^*}^* + \mathbf{v}^* \mathbf{u}_{\mathbf{y}^*}^* &= -\frac{\mathbf{p}_{\mathbf{x}^*}^*}{\rho^*}, \\ \mathbf{v}_{\mathbf{t}^*}^* + \mathbf{u}^* \mathbf{v}_{\mathbf{x}^*}^* + \mathbf{v}^* \mathbf{v}_{\mathbf{y}^*}^* &= -\frac{\mathbf{p}_{\mathbf{y}^*}^*}{\rho^*} - \mathbf{g}; \end{aligned}$$

at the free surface  $\mathbf{y}^* = \eta^*$ ,

$$\eta_{\mathbf{t}^*}^* + \mathbf{u}^* \eta_{\mathbf{x}^*}^* - \mathbf{v}^* = 0, \quad \mathbf{p}^* = -\mathbf{T} \eta_{\mathbf{x}^* \mathbf{x}^*}^* / (1 + (\eta_{\mathbf{x}^*}^*)^2)^{1/2};$$

at the rigid bottom  $\mathbf{y}^* = -\mathbf{h} + \mathbf{b}^*(\mathbf{x}^*)$ ,

$$\mathbf{u}^* \mathbf{b}_{\mathbf{x}^*}^* - \mathbf{v}^* = 0;$$

as  $x^* \rightarrow -\infty$ ,  $(\mathbf{u}^*, \mathbf{v}^*) \rightarrow (C, 0)$ , where  $(\mathbf{u}^*, \mathbf{v}^*)$  is the velocity vector,  $\rho^*$  is the constant density of the fluid,  $y^* = \eta^*(x^*, t^*)$  is the equation of the free surface,  $p^*$  is the pressure, and  $g$  is the gravity constant. Here,  $\mathbf{b}^*(x^*)$  stands for the bump of finite support on the rigid horizontal bottom,  $h$  is the depth of the fluid at far upstream, and  $T$  is the surface tension coefficient on the free surface.

To non-dimensionalise, the following dimensionless variables are used:

$$\begin{aligned} \epsilon^{1/2} &= (h/L), \quad (x, y) = (\epsilon^{1/2}x^*/h, y^*/h), \\ t &= \epsilon^{5/2}\sqrt{g/h}t^*, \quad \tau = T/(\rho^*gh^2), \\ (\mathbf{u}, \mathbf{v}) &= (\mathbf{u}^*, \epsilon^{-1/2}\mathbf{v}^*)/\sqrt{gh}, \quad p = p^*/(gh\rho^*), \\ \eta &= \epsilon^2\eta^*/h, \quad b(x) = \mathbf{b}^*(x^*)/(h\epsilon^4), \end{aligned}$$

where  $L$  is the horizontal length scale.

In terms of the above non-dimensional variables and by assuming that  $\mathbf{u}, \mathbf{v}, p$  and  $\eta$  possess an asymptotic expansion of the form

$$\phi = \phi_0 + \epsilon\phi_1 + \epsilon^2\phi_2 + \dots,$$

with  $\mathbf{u}_0 = 1, \mathbf{v}_0 = 0, p_0 = -y + 1$  and the upstream Froude number  $F = C/(gH^*)^{1/2} = 1 + \epsilon^2\lambda_1$ , boundary conditions and a system of differential equations for successive approximations are obtained according to the order of  $\epsilon$ . Then, by solving the resulting equations with the assumptions that  $\eta(-\infty) = \eta_x(-\infty) = \eta_{xx}(-\infty) = \eta_{xxx}(-\infty) = 0$ , the following F-Kawahara equation is derived when  $\tau = 1/3 + \tau_1\epsilon$ . The details of this derivation are given in [6].

$$\eta_t + \lambda_1\eta_x + (\tau_1/2)\eta_{xxx} - (3/2)\eta\eta_x - (1/90)\eta_{xxxx} - (1/2)\mathbf{b}_x = 0. \quad (5)$$

In the following, we will study the solutions of (3) theoretically and numerically.

### 3 Steady F-Kawahara equation for $\lambda_1 < 0$

In this section, we consider the steady F-Kawahara equation (4) and its solutions that tend to zero at both plus and minus infinity. Integrating (4) from  $-\infty$  to  $x$  with  $\eta(-\infty) = \eta_x(-\infty) = \eta_{xx}(-\infty) = \eta_{xxx}(-\infty) = 0$ , we obtain

$$2\lambda_1\eta + \tau_1\eta_{xx} - (3/2)\eta^2 - (1/45)\eta_{xxxx} = b(x). \quad (6)$$

In the following, we assume that  $b(x)$  is even function of  $x$  and has a compact support.

First, we consider the linear equation

$$2\lambda_1\eta + \tau_1\eta_{xx} - (1/45)\eta_{xxxx} = 0. \quad (7)$$

If  $\lambda_1 > 0$ , there are two real eigenvalues and two purely imaginary eigenvalues, which corresponds to a saddle-center phase space. If  $\lambda_1 < 0$ , then there are three cases: for  $-(\tau_1/2)\sqrt{90/|\lambda_1|} < -2$ , there are four real eigenvalues; for  $-2 < -(\tau_1/2)\sqrt{90/|\lambda_1|} < 2$ , there are two pairs of complex conjugate eigenvalues; for  $-(\tau_1/2)\sqrt{90/|\lambda_1|} > 2$ , there are two pairs of purely imaginary eigenvalues. When  $\lambda_1 < 0$  and  $-(\tau_1/2)\sqrt{90/|\lambda_1|} \leq -2$ , there is a unique solitary-wave solution decaying exponentially at infinity [4]. For  $\lambda_1 < 0$  and  $-2 < -(\tau_1/2)\sqrt{90/|\lambda_1|} < 2$ , there are infinitely many solutions with exponentially decaying oscillations at infinity [4]. Based upon these linear and nonlinear results, we will only consider the case with  $\lambda_1 < 0$ , because non-decaying oscillations at infinity for  $\lambda_1 > 0$  may generate infinite energy for the solutions of time-dependent equations that seems not physically relevant. Hence, we assume that  $\lambda_1 < 0$  in the followings. For  $-(\tau_1/2)\sqrt{90/|\lambda_1|} < 2$ , for fixed  $\tau_1$  there exists a solution  $\eta$  of (6) which converges to zero as  $x \rightarrow \pm\infty$  if  $\lambda_1 < 0$  is large [6].

### 3.1 Symmetric steady solutions

Since in general we can not prove the existence of solutions of (6) near the nontrivial solutions of (2) found in [4], in the following, we use a numerical shooting method to find symmetric solutions of (6) when  $\mathbf{b}(x)$  is given by  $\mathbf{b}(x) = (1 - x^2)^{1/2}$  for  $|x| \leq 1$  and  $\mathbf{b}(x) = 0$  for  $|x| > 1$ .

The numerical method for calculating the solutions of (2) was carefully discussed in [4]. Here, we use a different shooting method for finding the numerical solutions of (6). We start with an initial value problem with the equation (6) and initial conditions  $\eta(-1) = \alpha_0, \eta'(-1) = \beta_0, \eta''(-1) = \gamma_0$  and  $\eta'''(-1) = \beta_0^{-1}((1/2)\gamma_0^2 - \lambda_1\alpha_0^2 + (1/3)\alpha_0^3 - (\tau_1/2)\beta_0^2)$ , where the condition on  $\eta'''(-1)$  is derived from the zero condition of the solution at  $-\infty$ . Then, for a fixed  $\alpha_0$ , we use an initial choice of  $(\beta_0, \gamma_0)$  and apply the Runge-Kutta method to find the solution of the initial value problem, which gives  $f_0(\beta_0, \gamma_0) = \eta'(0)$  and  $g_0(\beta_0, \gamma_0) = \eta'''(0)$  (of course, with some bad choice of  $\alpha_0, \beta_0, \gamma_0$ , the solution may blow up before reaching  $x = 0$ ). Then, we apply Newton's iteration to find  $\beta_{0,n+1}$  and  $\gamma_{0,n+1}$  until  $\max(|f_0(\beta_{0,n+1}, \gamma_{0,n+1})|, |g_0(\beta_{0,n+1}, \gamma_{0,n+1})|) < 10^{-6}$ , where  $f_0$  and  $g_0$  are found using the Runge-Kutta method. After finding  $\beta_0, \gamma_0$ , we use the initial condition with this  $(\alpha_0, \beta_0, \gamma_0)$  to calculate the solution further for  $x = 100$  and make sure the solution approaching to zero by varying  $\alpha_0$ . Then, from the evenness of the solution, the solution of (6) can be numerically obtained for  $x \in [-100, 100]$ .

By the shooting method discussed above, we fix the value of  $\tau_1$  and let  $\lambda_1 < 0$  vary so that the condition  $-(\tau_1/2)\sqrt{90/|\lambda_1|} < 2$  is satisfied. In our calculation,  $\tau_1 = 0.3$  and  $\tau_1 = -0.3$  are used.

From numerical computations, we find that two types of symmetric single-hump solutions and the solution branches are connected, which are shown in Figure 1. The top branch is for  $\eta_s$  and the lower one is for  $\eta_\ell$ . Here,  $\eta_s$  stands for small symmetric one-hump solution near zero and  $\eta_\ell$  is the larger symmetric one-hump solution. There are no single-hump solutions for

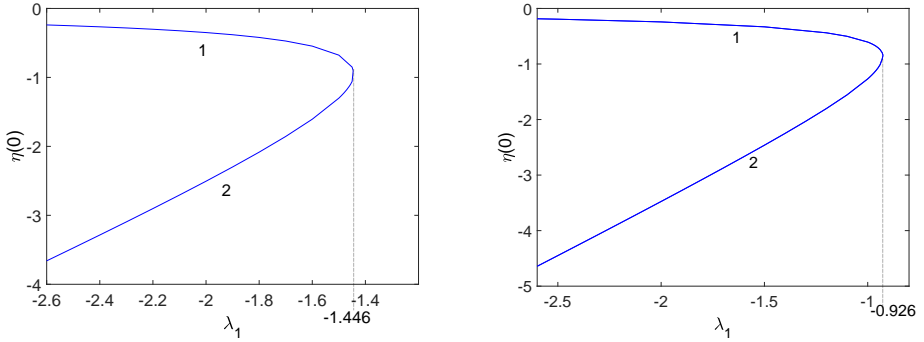


Figure 1: Branch curve for  $\eta_s$  and  $\eta_\ell$  for  $\tau_1 = -0.3$  and  $\tau_1 = 0.3$ .

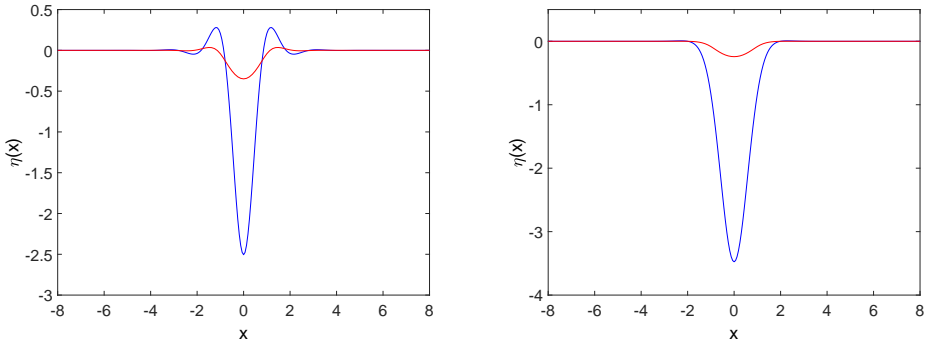


Figure 2: Typical  $\eta_s$  and  $\eta_\ell$  when  $\tau_1 = -0.3$  and  $\tau - 1 = 0.3$ .  $\lambda_1 = -2$  for both.

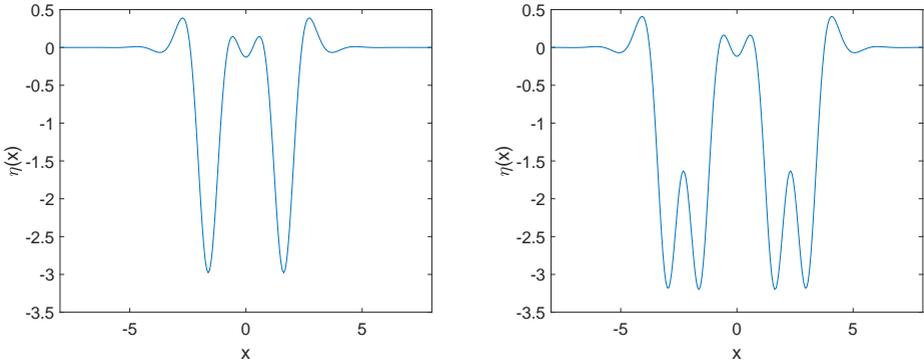


Figure 3: Typical two-hump solution and four-hump solution when  $\tau_1 = -0.3$  and  $\lambda_1 = -2$

$-1.446 < \lambda_1 < 0$  with  $\tau_1 = -0.3$  or  $-0.928 < \lambda_1 < 0$  with  $\tau_1 = 0.3$ .

The typical symmetric single-hump solutions  $\eta$  corresponding to  $\tau_1 = -0.3$ ,  $\lambda_1 = -2$  and to  $\tau_1 = 0.3$ ,  $\lambda_1 = -2$  are shown in Figure 2 (only the solution curves for  $x \in [-8, 8]$  are shown although the calculations are carried out for  $x \in [-100, 100]$ ).

Moreover, since (2) has infinitely many solutions for  $\lambda_1 = -2$ ,  $\tau_1 = \pm 0.3$ , we expect that there would be other solutions of (6) that are near solutions of (2). Indeed, there exist many different types of solutions of (6), some of which are given in Figure 3 and Figure 4. Two-hump solutions and four-hump solutions are found numerically for  $\tau_1 = -0.3$  and three-hump and five-hump solutions are found numerically for  $\tau_1 = 0.3$ . Figure 3 shows two-hump solution and four-hump solutions and three-hump solution and five-hump solutions are given in Figure 4.

In Figure 5, the bifurcation curves for two-hump solutions and three-hump solutions are provided. The two-hump solutions only exist for  $\lambda_1 < -1.027$  for  $\tau_1 = -0.3$  and the three-hump solutions exist for  $\lambda_1 < -0.926$  for  $\tau_1 = 0.3$ .

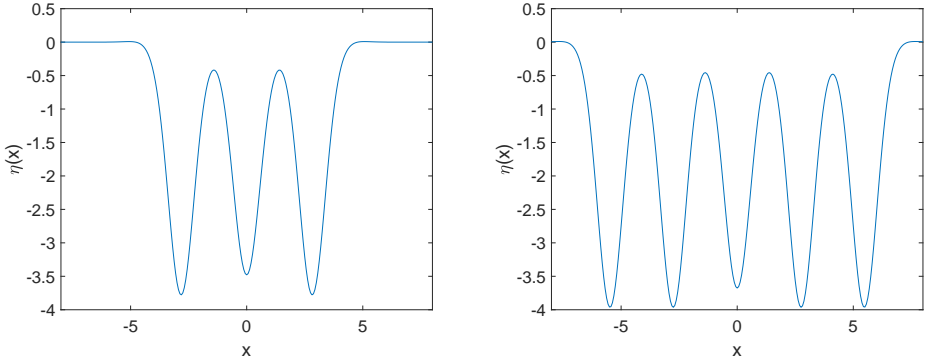


Figure 4: Typical three-hump solution and five-hump solution when  $\tau_1 = 0.3$  and  $\lambda_1 = -2$

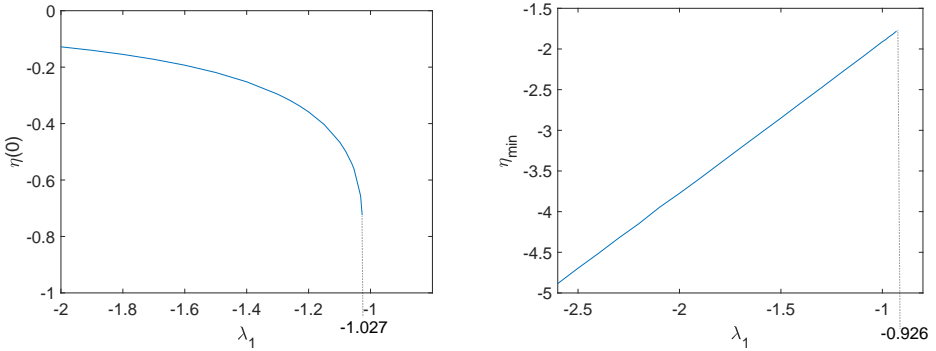


Figure 5: Branch curve of two-hump solutions for  $\tau_1 = -0.3$  and three-hump solutions for  $\tau_1 = 0.3$ .

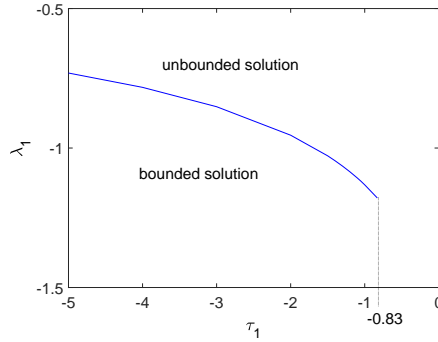


Figure 6: The branch curve of  $\lambda_c$  for hydraulic fall solutions.

### 3.2 Hydraulic fall solutions

For  $-\tau_1 \sqrt{90/|\lambda_1|}/2 > 2$ , symmetric steady solutions of (6) could not be found but hydraulic fall solutions were found numerically as the limiting solutions of bounded periodic wave solutions. To find hydraulic fall solutions of (6) we solve (6) by the Runge-Kutta Method with the assumption  $\eta = 0$  for  $(-\infty, -1)$ . The numerical results are given in Figure 6 and Figure 7. For a given  $\tau_1$  there exists corresponding critical  $\lambda_c$  less than which bounded solutions exist. If  $\lambda_1 > \lambda_c$  the solution becomes unbounded. The hydraulic fall solution is obtained when  $\lambda_1 = \lambda_c$ . We note that hydraulic fall solutions appear numerically for  $\tau_1 < -0.83$ . The relation between  $\tau_1$  and  $\lambda_c$  is given in Figure 6. Figure 7 shows a typical hydraulic fall solution and a typical bounded solution for  $\tau_1 = -4$  respectively.

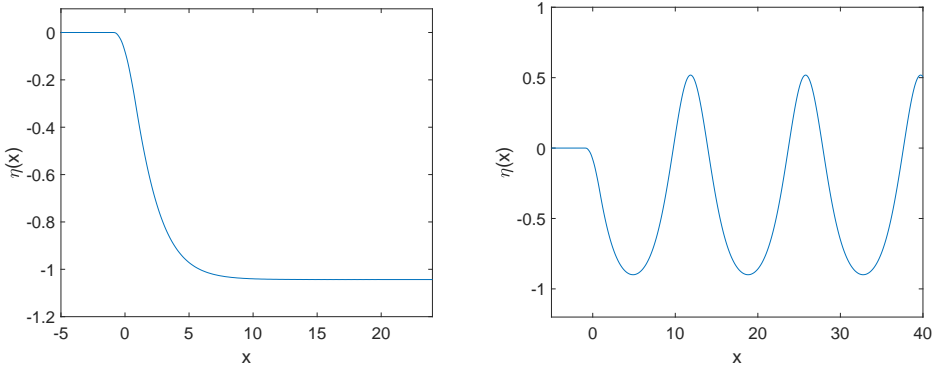


Figure 7: Typical hydraulic fall solution with  $\tau_1 = -4$  and  $\lambda_1 = -0.78250686$  and typical bounded solution with  $\tau_1 = -4$  and  $\lambda_1 = -0.8$ .

## 4 Stability of steady-state solutions and time evolutions of zero wave

In this section, we first consider the stability of the steady-state solutions found in Section 3 numerically. It has been noted that there are many different types of steady solutions. However, in real physical situations, only stable solutions can be observed. The global well-posedness of the initial value problem for arbitrary initial condition  $\eta_0(x)$  in  $H^2(\mathbf{R})$  and stability analysis has been carried out rigorously by Choi, Whang, and Sun in [6] and the solution of (3) with  $\eta(x, 0)$  in  $H^2(\mathbf{R})$  exists for  $t \in [0, +\infty)$ . In the following, we investigate the numerical stability of steady-state solutions in Subsection 4.1. In Subsection 4.2, we investigate the time evolutions of zero wave.

## 4.1 Numerical stability of steady-state solutions

In this subsection we investigate numerically the long-time behavior of solutions of (3) for the initial conditions  $\eta(\mathbf{x}, 0)$  near the steady-state solutions of (6) obtained in Section 3, where the forcing term  $\mathbf{b}(\mathbf{x})$  is the one used in Section 3. To find the solutions of the IVP (3) with  $\eta(\mathbf{x}, 0)$  numerically, we use a generalised Crank-Nicolson scheme to discretise the temporal variable and we apply the discretised fast Fourier transform method for the spatial variable. For the spatial variable, we use the periodic boundary conditions. For more detailed discussion on this method, see the book by Trefethen [16]. The interval considered in the numerical calculation is  $-100 \leq \mathbf{x} \leq 100$ . The temporal and spatial steps are  $10^{-4}$  and  $10^{-2}$ , respectively. For the computation of the fast Fourier transforms, MATLAB software was used.

As was pointed out in Section 3, it is known that for a fixed  $\tau_1 = -0.3$  there is a cut-off value  $\lambda_0 \sim -1.446$  for  $\lambda_1$  such that there are two symmetric single-hump solutions  $\eta_s$  and  $\eta_t$  of (6) for each  $\lambda_1 < \lambda_0$  and no steady single-hump solutions for  $0 > \lambda_1 > \lambda_0$ . Also, there are many multi-hump solutions for certain values of  $\lambda_1 < 0$ . We numerically study the stability and instability of these solutions. When the initial data  $\eta(\mathbf{x}, 0)$  is close to either  $\eta_s$  or  $\eta_t$ , the behavior of solution of (3) with  $\eta(\mathbf{x}, 0)$  is investigated as time evolves.

First, let us consider the stability of  $\eta_s$ . In Subsection 4.2, we know that for large  $\lambda_1 < 0$ ,  $\eta_s$  is stable. The numerical results of (3) for this case are obtained when the initial conditions  $\eta(\mathbf{x}, 0)$  are taken as  $\eta_s$  plus small computer noise. The numerical results are given in the first figure of Figure 8. The figure shows the time evolution of the solution when  $\lambda_1 = -2$  and  $\tau_1 = -0.3$ . As is shown in the figures, when time tends to infinity, the solutions converges to  $\eta_s$ . Here, the actual numerical computation is accomplished for  $-100 \leq \mathbf{x} \leq 100$ . The same phenomena happen for all values of  $\lambda_1$  such that  $\eta_s$  exists.

The instability of  $\eta_t$  for (3) is shown in the second figure of Figure 8. The initial conditions are chosen as  $\eta_t$  plus computational noise with a 5% perturbation. The time evolution of the solution of (3) is shown in Figure 9

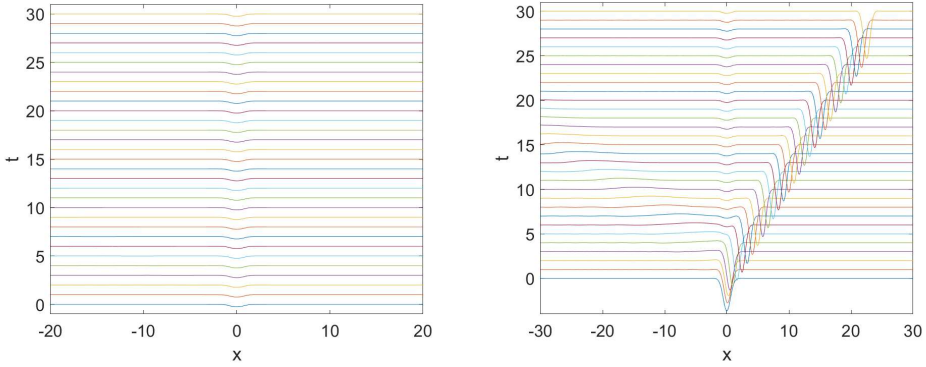


Figure 8: Time evolution of  $\eta_s$  and  $\eta_\ell$  with 5% noise when  $\tau_1 = -0.3$ ,  $\lambda_1 = -2$ .

in this case for  $\lambda_1 = -2$  and  $\tau_1 = -0.3$ . When the total perturbation is positive, the amplitude of the solution becomes larger as time increases and a traveling single-hump wave is generated after a certain time and moves to the downstream. As time evolves, the traveling single-hump wave propagates apart from the bump and the small steady solution  $\eta_s$  appears above the bump, which is stable. Moreover, if the total perturbation is negative, the same phenomenon holds except that the traveling single-hump wave moves to the upstream. Such phenomena happen to all cases of  $\lambda_1$  for which  $\eta_\ell$  exists. Thus, for each  $\lambda_1 < \lambda_0 < 0$ , a traveling single-hump wave is generated after a certain time and moves to upstream or downstream and a stable wave with small amplitude appears over the top of the bump.

The instability of five-hump solutions for (3) is shown in Figure 9. The initial conditions are chosen as the five-hump solution obtained in Section 3 plus 5% noise. In this case for  $\lambda_1 = -2$  and  $\tau_1 = -0.3$ . It can be seen that the five-hump solution is unstable, although it may stay in its position for a quite some time. We note that the instability of other multi-hump solutions similar to that of five-hump solution.

The time evolution of the hydraulic fall solution is also given in Figure 10.

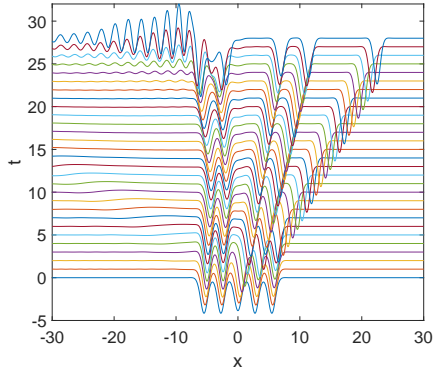


Figure 9: Time evolution of the five-hump solution with 5% noise when  $\tau_1 = 0.3, \lambda_1 = -2$ .

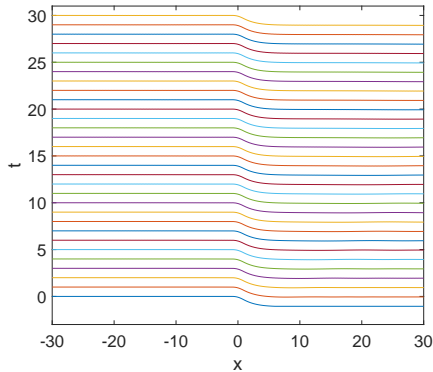


Figure 10: Time evolution of hydraulic fall solution with 5% noise when  $\tau_1 = -4, \lambda_1 = -0.78250686$ .

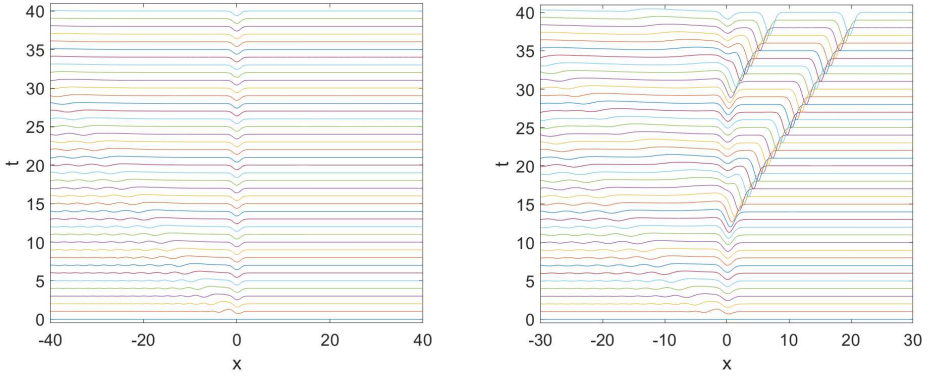


Figure 11: Time evolution of zero wave when  $\tau_1 = 0.3$  with  $\lambda_1 = -1$  and  $\lambda_1 = -0.8$  respectively.

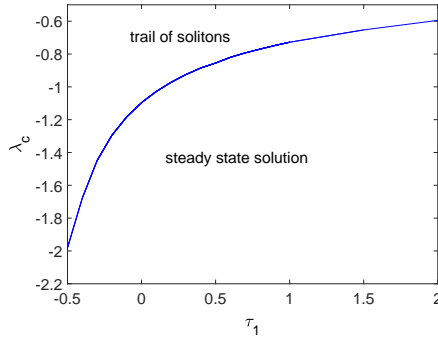


Figure 12: The relationship between  $\tau_1$  and  $\lambda_c$ .

The initial condition is given as the hydraulic fall solution in Section 3. With computational noise and 5% perturbation, as time tends to infinity, the solutions converges to the hydraulic fall solutions. The same phenomena happen for all values of  $\lambda_1$  such that hydraulic fall solution exists.

## 4.2 Time evolution of the zero wave

In this subsection numerical solutions of (3) subject to the initial condition  $\eta(x, 0) \equiv 0$  are considered, where the forcing term  $b(x)$  is the one used in Section 3. The behaviours of the solutions are different for different values of  $\tau_1$  and  $\lambda_1$ . For a fixed  $\tau_1$  there exists corresponding critical  $\lambda_c$  such that if  $0 > \lambda_1 > \lambda_c$  a trail of solitary waves are generated and move upstream. If  $0 > \lambda_c > \lambda_1$  the solution converges to steady one-hump solution as time  $t$  tends to infinity. Figure 11 shows the time evolution of the solution of zero wave for  $\tau_1 = 0.3$  with  $\lambda_1 = -1$  and  $\lambda_1 = -0.8$ . The relation between  $\tau_1$  and  $\lambda_c$  is given in Figure 12.

## 5 Conclusion

In summary we consider physical problem of flow past a positive, symmetric body at the horizontal bottom of a fluid with surface tension at the free surface. The derivation of the forced KdV fails when Bond number  $\tau$  is near  $1/3$  and the following F-Kawahara equation is obtained.

$$\eta_t + \lambda_1 \eta_x - (3/2)\eta\eta_x + (\tau_1/2)\eta_{xxx} - (1/90)\eta_{xxxxx} = b_x/2,$$

$$x \in (-\infty, +\infty), \quad t > 0,$$

which describes the long wave approximations of the solutions of exact equations for a two dimensional fluid in the critical cases that the upstream Froude number  $F = C/(gH^*)^{1/2}$  is near 1 and Bond number  $\tau$  is near  $1/3$ . The F-Kawahara equation possesses various types of steady-state solutions. Two parameters appear in the equation and can affect its solution behaviour. One is the parameter  $\lambda_1$ , a measure of the deviation of the flow speed at far upstream from the 1, and the other is the difference  $\tau - 1/3 = \tau_1$ . Mathematically different types of steady solutions which may appear in different regions of the  $\lambda_1 - \tau_1$  plane were discovered and their numerical stabilities were also studied. One may expect that only stable solutions are observable in nature

and the unstable solutions are much harder to observe. This investigation may help us understand the flow patterns under parameter change in a fluid with obstructions at boundaries.

## References

- [1] B. Buffoni. Infinitely many large amplitude homoclinic orbits for a class of autonomous hamiltonian systems. *J. Differential Equations* (121):109–120, 1995. doi:[10.1006/jdeq.1995.1123](https://doi.org/10.1006/jdeq.1995.1123) C78, C79
- [2] B. Buffoni and J. F. Toland. Global existence of homoclinic and periodic orbits for a class of autonomous hamiltonian systems. *J. Differential Equations*, (118):104–120, 1995. doi:[10.1006/jdeq.1995.1068](https://doi.org/10.1006/jdeq.1995.1068) C78, C79
- [3] A. V. Buryak and A. R. Champneys. On the stability of solitary wave solutions of the fifth-order kdv equation. *Phys. Lett. A*, (233):58–62, 1997. doi:[10.1016/S0375-9601\(97\)00453-2](https://doi.org/10.1016/S0375-9601(97)00453-2) C78, C79
- [4] A. R. Champneys and J. F. Toland. Bifurcation of a plethora of multi-modal homoclinic orbits for autonomous hamiltonian systems. *Nonlinearity*, (6):665–721, 1993. C78, C79, C82, C83
- [5] J. W. Choi, S. M. Sun, and M. C. Shen. Steady capillary-gravity waves on the interface of two-layer fluid over an obstruction-forced modified k-dv equation. *J. Eng. Math.*, (28):193–210, 1994. doi:[10.1007/BF00058436](https://doi.org/10.1007/BF00058436) C78
- [6] J. W. Choi, S. M. Sun, and S. I. Whang. Steady surface waves on water over a bump with critical surface tension. *accepted*. C79, C81, C82, C88
- [7] J. W. Choi, S. M. Sun, and S. I. Whang. Supercritical surface gravity waves generated by a positive forcing. *European J. Mech. B/Fluids*, (27):750–770, 2008. doi:[10.1016/j.euromechflu.2008.01.006](https://doi.org/10.1016/j.euromechflu.2008.01.006) C78

- [8] L. K. Forbes. Critical free surface flow over a semi-circular obstruction. *J. Eng. Math.*, (22):3–13, 1988. doi:[10.1007/BF00044362](https://doi.org/10.1007/BF00044362) C78
- [9] J. Hunter and J. Scheurle. Existence of perturbed solitary wave solutions to a model equation for water waves. *Phys. D*, (32):253–268, 1988. doi:[10.1016/0167-2789\(88\)90054-1](https://doi.org/10.1016/0167-2789(88)90054-1) C78, C79
- [10] J.K Hunter and J.M. Vanden-Broeck. Solitary and periodic gravity-capillary waves of finite amplitude. *J. Fluid Mech.*, (134):205–219, 1983. doi:[10.1017/S0022112083003316](https://doi.org/10.1017/S0022112083003316) C78
- [11] T. Iguchi. A mathematical justification of the forced korteweg-de vries equation for capillary-gravity waves. *Kyushu Journal of Mathematics*, 60(2):267–303, 2006. doi:[10.2206/kyushujm.60.267](https://doi.org/10.2206/kyushujm.60.267) C78
- [12] J. W. Miles. Stationary, transcritical channel flows. *J. Fluid Mech.*, (162):489–499, 1986. doi:[10.1017/S0022112086002136](https://doi.org/10.1017/S0022112086002136) C78
- [13] Y. Pomeau, A. Ramani, and B. Grammaticos. Structural stability of the korteweg-de vries solitons under a singular perturbation. *Phys. D*, (31):127–134, 1988. doi:[10.1016/0167-2789\(88\)90018-8](https://doi.org/10.1016/0167-2789(88)90018-8) C78, C79
- [14] J. J. Stoker. *Water Waves: The Mathematical Theory with Applications*. *Pure and Applied Mathematics, Interscience Publishers, Inc., New York*, 4 edition, 1957. C78, C80
- [15] S. M. Sun and M. C. Shen. Exponentially small estimate for a generalized solitary wave solution to the perturbed k-dv equation. *Nonlinear Anal.*, (23):545–564, 1994. doi:[10.1016/0362-546X\(94\)90093-0](https://doi.org/10.1016/0362-546X(94)90093-0) C78, C79
- [16] L. N. Trefethen. *Spectral Methods in MATLAB*. *SIAM, Philadelphia, PA*, 2003. C89
- [17] J. M. Vanden-Broeck. Free surface flow over a semi-circular obstruction in a channel. *Phys. Fluids*, (30):2315–2317, 1987. C78

## Author addresses

1. **JS Kim**, Department of Mathematics, Korea University, Seoul, Korea.
2. **SI Whang**, Department of Mathematics, Ajou University, Suwon, Korea.
3. **JW Choi**, Department of Mathematics, Korea University, Seoul, Korea.